power divider incorporating $\lambda/4$ transformers is properly designed to feed the array elements. The elements of the array are spaced at a distance of $0.8\lambda_0$ from each other in both x- and y-directions.

4.2. Simulated and Measured Results

The 2×2 planar array resonates at 5.45 GHz with simulated S_{11} being -29.2 dB and having an impedance bandwidth of 48 MHz. The measured value of S_{11} is found to be -20.1 dB at 5.47 GHz and the comparative results are shown in Figure 10(c). The simulated and measured radiation patterns for E-plane and H-plane are plotted in Figures 11(a) and 11(b), respectively. For E-plane, the simulated and measured co-polarization gains obtained are 9.6 dBi and 9.4 dBi respectively while for H-plane the corresponding values are 9.6 dBi and 9.5 dBi, respectively. It is thus evident that for 2×2 planar array the gain increases from 5.7 to 9.6 dBi as compared to a single array element. Its maximum radiation is in the direction of $\theta = -10^\circ$ with 91% radiation efficiency.

5. CONCLUSION

A SIW based equilateral triangular antenna is proposed which produces a gain of 5.7 dBi. Based on this element, linear and planar antenna arrays have been designed at 5.4 GHz band, fabricated and their various parameters being studied extensively. The presence of PEC walls on two sides of the array elements reduces mutual coupling between the two elements thereby allowing design of compact arrays. The primary objective of gain enhancement using arrays has been successfully realized. For the 1×2, 1×4 and 2×2 arrays the corresponding gains are 7.5 dBi, 10.7 dBi, and 9.6 dBi which are much more as compared to the single array element with 5.7 dBi gain. The antenna arrays at the canopy 5.4 GHz unlicensed band will go a long way to satisfy the needs of the users for WiFi access, high speed wireless broadband services and cordless telephone applications.

REFERENCES

1. D. Deslandes and K. Wu, Accurate modeling, wave mechanisms and design considerations of a substrate integrated waveguide, IEEE Trans Microwave Theory Tech 54 (2006), 2516–2526.
2. F. Xu and K. Wu, Guided-wave and leakage characteristics of substrate integrated waveguide, IEEE Trans Microwave Theory Tech 53 (2005), 66–73.
3. L. Yan, W. Hong, G. Hua, J.X. Chen, K. Wu, and T.J. Cui, Simulation and experiment on SIW slit array antennas, IEEE Microwave Wireless Compon Lett 14 (2004), 446–448.
4. P. Chen, W. Hong, Z.Q. Kuai, and J. Xu, A substrate integrated waveguide circular polarized slot radiator and its linear array, IEEE Antennas Wireless Propag Lett 8 (2009), 120–123.
5. D.M. Pozar, Microwave engineering, 3rd ed., Wiley, New York, NY, USA, 2005.
6. J.S. Hong and S. Li, Theory and experiment of dual-mode microstrip triangular patch resonators and filters, IEEE Trans Microwave Theory Tech 52 (2004), 1237–1243.
7. Q. LaiCh. Fumeaux, W. Hong, and R. Vahldieck, Characterization of the propagation properties of the Half-mode substrate integrated waveguide, IEEE Trans Microwave Theory Tech 57 (2009), 1996–2004.
8. T. Sauer, Numerical analysis, Upper Saddle River, NJ, USA, Pearson Educ, 2006.

ACETONE EVAPORATION AND WATER VAPOR DETECTION USING A CATERPILLAR-LIKE MICROSTRUCTURED FIBER

A. D. Gomes,[1,2] M. F. S. Ferreira,[1,2] J. P. Moura,[1] R. M. André,[1,2,3] J. Kobelke,[3] J. Bierlich,[3] K. Wondraczek,[3] K. Schuster,[3] and O. Frazão[1,2]

[1] INESC TEC and Department of Physics and Astronomy, Faculty of Sciences, University of Porto, Rua Do Campo Alegre 687, Porto 4169-007, Portugal

[2] Department of Physics and Astronomy, Faculty of Sciences, University of Porto, Rua Do Campo Alegre 687, Porto 4169-007, Portugal

[3] Leibniz Institute of Photonic Technology (IPHT Jena), Albert-Einstein-Straße 9, Jena 07745, Germany

Received 14 July 2015

ABSTRACT: *A new microstructured optical fiber is presented as a sensor of acetone evaporation. Sensing is performed by observing the time response of the reflected signal at 1550 nm when the device is dipped in acetone or a 50% acetone–50% water mixture. The sensor consists on a caterpillar-like microstructured fiber spliced to a single-mode fiber, where the spliced end of the sensor has a transversal microfluidic channel etched using focused ion beam. Upon heating, different behaviors are visible between the dipping and the evaporation of acetone. The sensor is able to track the evaporation of acetone and to distinguish between pure acetone and a 50% acetone–50% water mixture. The sensor is also able to detect when the acetone in a mixture with water is fully evaporated. The detection of water vapor with no particular orientation of the sensor is achieved due to the presence of the microfluidic channels.* © 2016 Wiley Periodicals, Inc. Microwave Opt Technol Lett 58:679–683, 2016; View this article online at wileyonlinelibrary.com. DOI 10.1002/mop.29644

Key words: *optical fiber sensor; microstructured fiber; evaporation of acetone; water vapor*

1. INTRODUCTION

The interaction between the evanescent field and fluids inserted into microstructured optical fiber holes has been the object of extensive research for sensing purposes. This concept led to several reported fiber designs for the sensing of trace elements in gases and liquids [1–4] Further investigations have been developed using this interaction to monitor the evaporation of volatile organic compounds. Some configurations for this purpose have been recently studied, namely, with suspended-core optical fibers (SCFs) [5], microstructured optical fibers (MOFs) [6] and fiber-optic micro-cell cavities [7].

The study of volatile organic compounds is very useful, mainly for industrial and environmental monitoring. In this work, a new fiber for monitoring the acetone evaporation and for water vapor detection is presented. The fiber is composed of a sensor head spliced to a single-mode fiber (SMF). The sensor head is a caterpillar-like MOF with microfluidic channels created using a Focused Ion Beam technique [8].

2. EXPERIMENTAL SETUP

Figure 1(a) shows the experimental setup for acetone evaporation detection. It consists in a broadband source with central wavelength of 1550 nm with a 100 nm bandwidth connected to an optical circulator to read the sensor response in reflection. The reflected signal was analyzed with an optical spectrum analyzer.

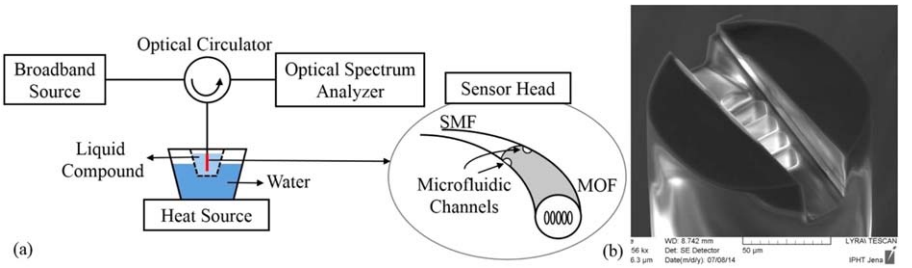

Figure 1 (a) Diagram of the experimental setup. (b) Cross section of the MOF with microfluidic channels. Image obtained by Scanning Electron Microscopy. [Color figure can be viewed in the online issue, which is available at wileyonlinelibrary.com]

The sensor head is a caterpillar-like MOF with ∼3 mm length. Transversal microfluidic channels were created at one end of the fiber using a focused ion beam technique and then spliced into a SMF. A cross section of the microfluidic channels is shown in Figure 1(b). These microfluidic channels allow the liquid within the MOF to flow.

The sensor head was immersed vertically in a beaker with a liquid volatile organic compound (acetone or a mixture of 50% acetone–50% water) at room temperature. The reservoir temperature was progressively increased in a bain-marie until the evaporation point of the volatile compounds (∼56°C for acetone [9] and 100°C for water). The time response of the reflected signal from the sensor head was analyzed at 1550 nm since the sensor is dipped in the reservoir until the complete evaporation of the liquid compounds inside the fiber.

From this setup some problems arise. First, the liquid compound was poured manually so, depending on the speed at which the liquid is poured, the response of the sensor varies. Second, during that process, the sensor head might touch the edges of the reservoir. Consequently, perfect reproducibility during this part could not be achieved.

For the water vapor detection, some changes in the setup were made. The beaker was removed from the setup leaving only the reservoir with water and the fiber was placed above it. Two modes of detection were considered: an horizontal detection, where the fiber is parallel to the water surface [Fig. 2(a)], and a vertical detection, where the fiber is perpendicular to the water surface [Fig. 2(b)], suspended above the water for both cases.

3. RESULTS

3.1. Acetone

The response of the sensor head to the evaporation process can be divided into four different stages, represented in Figure 3. The sensor head in air, without being in contact with the liquid, has a high and stable intensity value of the reflected signal. During the dipping process in acetone at room temperature [Fig. 3(a)], the liquid enters inside the sensor head holes causing an increase in transmitted light. Hence, a considerable drop (∼10dB) in the reflected signal is observed. A relatively high oscillation is observed while the sensor head is immersed in acetone at room temperature, as shown in Figures 3(a) and 3(b). During the heating process, this oscillation decreases and converges to around −36dB, near the boiling point (∼56°C) [Fig. 3(c)]. During the evaporation [Fig. 3(d)], the reflected signal starts fluctuating around −36dB. When no acetone is present outside the sensor head, the air begins to fill the sensor head holes and the reflected signal rises to the initial value of approximately −23dB.

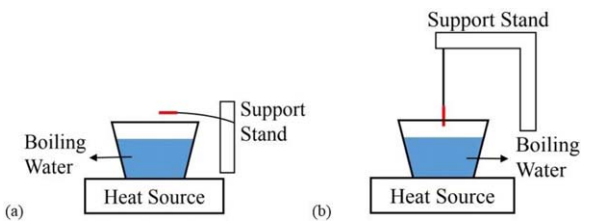

Figure 2 Diagram of the experimental setup for water vapor detection: (a) Horizontal detection, (b) Vertical detection. [Color figure can be viewed in the online issue, which is available at wileyonlinelibrary.com]

The drop in the reflected signal near the 5 seconds, in Figure 3(d), might be the result of liquid acetone moving inside the sensor head until it evaporates completely. It may also be due to acetone vapor that has condensed in the sensor head, because there is still acetone to evaporate in the container bottom when there is no longer contact between the sensor head and the acetone.

3.2. Mixture of 50% Acetone–50% Water

The response from the sensor head to the evaporation process of a 50% acetone–50% water mixture was also analyzed and can be divided into four different stages, represented in Figure 4. During the dipping process in the mixture at room temperature [Fig. 4(a)], the reflected signal decreases considerably (∼14dB), as in acetone in Figure 3(a), but is followed by a much faster oscillation with less amplitude. Shortly after dipping the sensor head into the mixture, the oscillation decreases and converges to around −37dB [Fig. 4(b)]. With increasing temperature, acetone evaporates and the sensor head remains immersed only in water. The reflected signal of the sensor head immersed in the water is around −32dB, as shown in Figure 4(c). As the water evaporation is slow, the sensor head was manually removed from the container. However, there was still water within the sensor head. The sensor head was placed near the heat source so that the water in its holes could evaporate. The water evaporation can be seen in Figure 4(d). High amplitude oscillations of the reflected signal are observed right before all the water within the sensor head evaporates. Although the sensor was being manually held, the high amplitude oscillations started only when the sensor was near the heat source. In the case of pure acetone [Fig. 3(d)], the evaporation inside the fiber holes is almost instantaneous, corresponding to the jump of the signal from around −35dB, where the holes are filled with acetone, to around −24dB, where no acetone is present and the holes are filled with air. In water, the evaporation process inside the fiber holes is not as fast as in acetone. This evaporation of the water inside the fiber holes is translated by the high oscillations from −32dB, where the fiber holes are filled with water, until the full

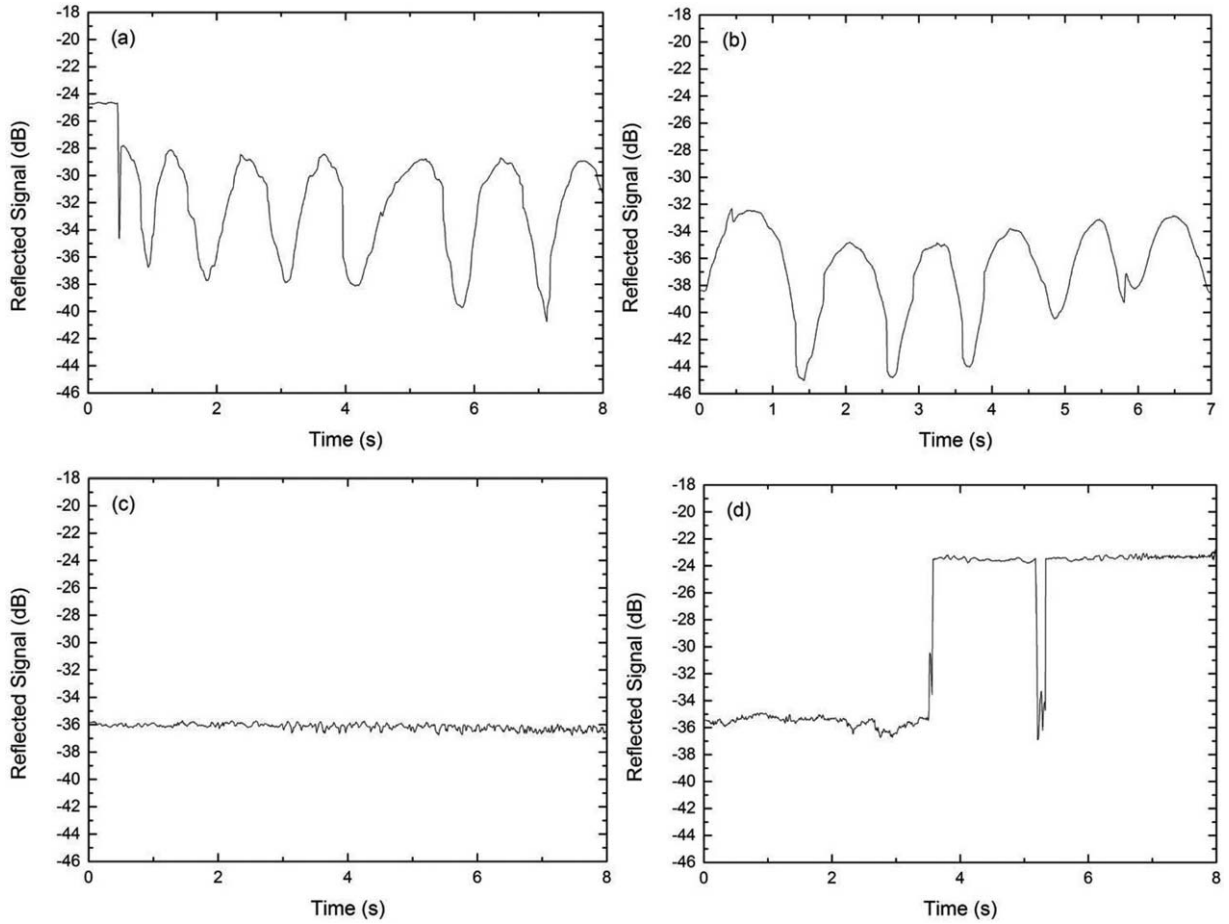

Figure 3 Time response of the reflected signal of the sensor head during the evaporation process of acetone: (a) dipping in room temperature acetone, (b) immersed in room temperature acetone, (c) immersed in acetone near the boiling point (~56°C) [9], (d) acetone evaporation.

evaporation of the water in the sensor head is achieved, represented by the rise of the reflected signal to around −20dB [Fig. 4(d)].

3.3. Water Vapor

The device was also sensitive to the presence of water vapor. This led to the study of the reflected signal time response in its presence. Falls and rises from the reflected signal were observed [Figs. 5 and 6]. The water vapor condenses in the fiber, causing more light to be transmitted and leading to a decrease in the reflected signal. As the water inside the fiber evaporates, the signal rises again. Two modes of detection were considered: horizontal and vertical, as shown next.

3.4. Horizontal

The fiber was fixed on a support stand above the reservoir so that it was horizontal, taking into account the curvature of the fiber due to its weight. With the water boiling, the fiber, initially away from the reservoir, was placed horizontally above the reservoir. When the fiber was initially away from the reservoir, the reflected signal was approximately stable. Oscillations and peaks appeared in the reflected signal after the fiber was placed above the reservoir, as shown in Figure 5.

Three measurements at different heights were obtained. The initial height was measured ~2 cm. To avoid interference the later heights were not measured. Those heights are the result of a reduction in the amount of water inside the reservoir due to evaporation. Higher oscillations are visible in the reflected signal for the fiber with a higher height [Fig. 5, (Height = 3)]. However, we could not find a definite correlation between height and oscillation amplitude since other uncontrollable parameters could be at stake. For example, droplets condensed in the external part of the fiber may go inside and evaporate right after, creating higher peaks (>10dB) than the normal peaks of the reflected signal.

3.5. Vertical

The fiber was positioned vertically above the water as seen in Figure 2(b). This time the fiber was always in contact with the water vapor and inside the recipient. A drop in the signal is visible every time the vapor condensates inside the fiber, as shown in Figure 6. Again, three measurements at different heights were obtained.

As in the previous case, there seems to be no apparent correlation between the amplitude of the oscillations of the reflected signal at different heights.

4. CONCLUSION

The detection of acetone evaporation with the MOF dipped in acetone was achieved by observing the reflected signal at 1550 nm. The evaporation was also detected for a 50% acetone–50% water mixture. This detection was possible thanks to the microfluidic channels responsible for the circulation of the liquid inside the MOF. Not only that, a differentiation of several stages between the dipping and the evaporation was visible.

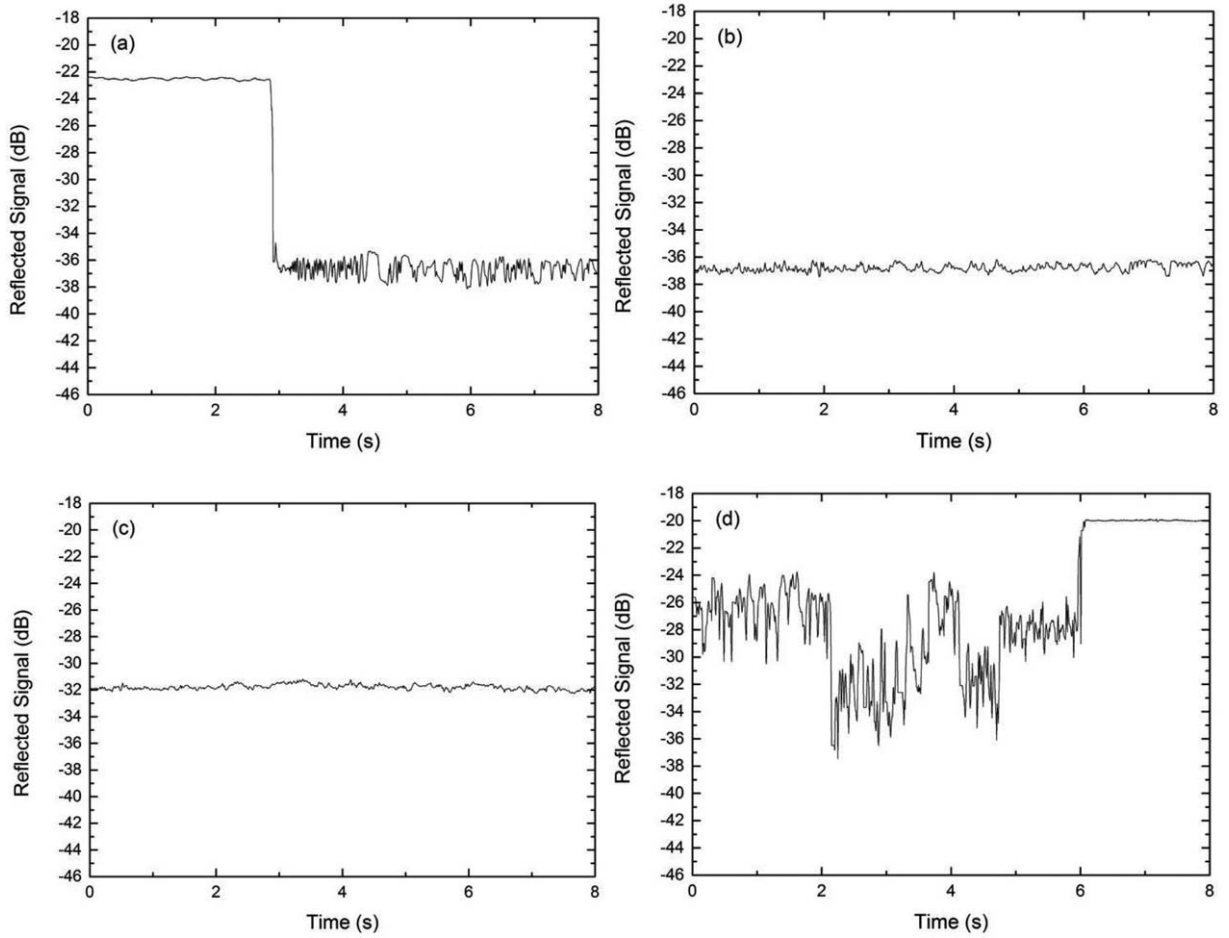

Figure 4 Time response of the reflected signal of the sensor head during the evaporation process of a 50% acetone–50% water mixture: (a) dipping in the mixture at room temperature, (b) immersed in the mixture at room temperature, (c) immersed in water, after all the acetone evaporated, (d) water evaporation.

The behavior of the signal in acetone at low temperatures differs to the one at near boiling temperatures. In the mixture, the acetone evaporation is visible with the rise of the signal's intensity, which could mean that this device would be able to differentiate the evaporation of substances with different properties from the same mixture.

Water evaporation was also detected. Placed above the water, the MOF was also able to detect the presence of water vapor in both horizontal and vertical configurations. In the horizontal configuration, higher oscillations were observed for higher heights, although the higher peaks may be caused by condensation droplets in the fiber and not by the height. This is supported by the vertical

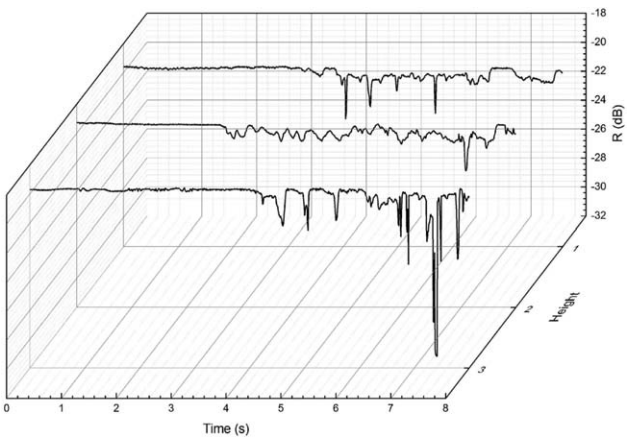

Figure 5 Time response of the reflected signal of the sensor head horizontal to the reservoir, when exposed to water vapor, at different heights: (1), (2) and (3), with (1)2.0cm < (2) < (3).

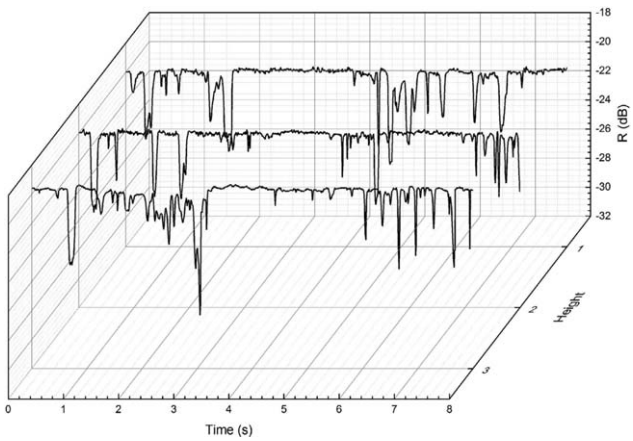

Figure 6 Time response of the reflected signal of the sensor head vertical to the reservoir, when exposed to water vapor, at different heights: (1), (2) and (3), with (1)1.0cm < (2) < (3).

configuration study, where no apparent relation between the intensity of the reflected signal and the height is visible.

Further studies should be handled to investigate the influence of the amount of condensation droplets in the outside part of the fiber during the water vapor detection. Automation of the dipping process as a future development would allow for more reproducible results.

REFERENCES

1. J.M. Fini, Microstructure fibres for optical sensing in gases and liquids, Meas Sci Technol 156 (2004), 1120–1128.
2. Y.L. Hoo,W. Jin, H.L. Ho, D.N. Wang, and R.S. Windeler, Evanescent-wave gas sensing using microstructure fiber, Opt Eng 411 (2002), 8–9.
3. T.M. Monro,W. Belardi, K. Furusawa, J.C. Baggett, N.G.R. Broderick, and D.J. Richardson, Sensing with microstructured optical fibres, Meas Sci Technol 127 (2001), 854–858.
4. G. Pickrell, W. Peng, and A. Wang, Random-hole optical fiber evanescent-wave gas sensing, Opt Lett 2913 (2004), 1476–1478.
5. J.P. Moura, H. Baierl, J.L. Auguste, R. Jamier, P. Roy, J.L. Santos, and O. Frazão, Evaporation of volatile compounds in suspended-core fibers, Opt Lett 39 (2014), 3868–3871.
6. S.O. Silva, J. Auguste, and R. Jamier, et al., Detection of evaporation process of acetone with a microstructured fiber in a reflective configuration, Opt Eng 53 (2014), 080501
7. E. Preter, B. Preloznik, V. Artel, C.N. Sukenik, D. Donlagic, and A. Zadok, Monitoring the evaporation of fluids from fiber-optic microcell cavities, Sensors 13 (2013), 15261–15273.
8. J.P. Moura, Microstructured Optical Fibers for Fluid Sensing Applications, M.S. Dissertation, University of Porto, Faculty of Sciences, (2014).
9. H.H. Amer, R.R. Paxton, and M.V. Winkle, Methanol-ethanol-acetone, Ind Eng Chem 48 (1956), 142–146.

SHORTING POSTS LOADED PATCH COUPLER WITH ENHANCED BANDWIDTH AND EXTENDED COUPLING COEFFICIENT RANGE

Bo Wei Xu,[1,2] Xing Yu Pu,[1,2] Shao Yong Zheng,[1,2] and Yun Liang Long[1,2]

[1] Department of Electronics and Communication Engineering, Sun Yat-Sen University, Guangzhou, China; Corresponding author: xmuzsy@hotmail.com

[2] SYSU-CMU Shunde International Joint Research Institute, Shunde, China

Received 16 July 2015

ABSTRACT: *This article presents a thorough investigation of the use of shorting posts to widen the bandwidth and coupling coefficient range of a patch quadrature coupler. The lumped equivalent circuit is used to analyze the characteristics of two proposed shorting posts loaded patch configurations. It is shown that by loading shorting post on the center of a patch, the bandwidth of coupler with loose coupling can be significantly improved. The patch configuration with four shoring posts is also proposed to provide a loose coupling coefficient up to 15 dB, which cannot be achieved using the conventional configuration. For demonstration purposes, two quadrature couplers were designed to exhibit 10 and 15 dB coupling coefficients with bandwidths of 29% and 19.2%, respectively.* © 2016 Wiley Periodicals, Inc. Microwave Opt Technol Lett 58:683–688, 2016; View this article online at wileyonlinelibrary.com. DOI 10.1002/mop.29643

Key words: *quadrature coupler; loose coupling; shorting post; wide band*

1. INTRODUCTION

Directional couplers are one of the important circuit components used in mixers, phase shifters, and amplifiers for wireless communication applications. To implement a directional coupler, a branch line coupler consisting of four quarter wavelength lines is usually employed [1]. Research on improving the performance of a coupler with equal power division ratio has been extensively conducted [2,3]. However, a coupler with loose coupling had been found to be useful in a power monitoring circuit by providing the appropriate amount of sampled power to a power detector. But for a branch-line coupler with loose coupling which is <10 dB, high-impedance lines are required. Therefore, the minimum coupling factor of the coupler is limited by the highest impedance of a pair of branch-lines that can be fabricated by general printed circuit board technologies. To overcome this problem, the defected ground structure was utilized underneath the microstrip line to realize high-impedance transmission line [4]. Alternatively, a pair of short-circuited coupled microstrip lines was employed to replace the conventional quarter wave length microstrip lines [5]. To implement a coupler for high-frequency applications, circular sector patch was proposed with simplicity in both design and fabrication alternatively [6]. Similar to other patch based circuits, the patch quadrature coupler suffers from a narrow operational bandwidth and large circuit size. Thus the patterned ground plane structure was introduced to solve the large circuit size problem without increasing circuit complexity [7]. As an extension, the varactor diodes are loaded on the patterned ground plane to implement frequency reconfiguration [8] for narrow bandwidth issue. Alternatively, the complementary split ring resonators can be loaded to implement a dual band quadrature coupler with different coupling coefficients [9]. However, the patch based quadrature coupler also exhibits the limitation in the implementation of loose coupling. The previous approaches [4,5] for micostrip line-based configuration cannot be applied to its patch based counterpart directly. Therefore, a new approach should be proposed to extend the bandwidth and coupling coefficient range for this class of quadrature coupler.

The introduction of shorting posts has received much attention in patch antennas. The applications include the frequency agility of microstrip patch antennas [10], impedance control of antennas [11], improvement of scanning range of patch arrays [12], and reducing of the surface wave effects in a patch element [13]. Compared to other techniques, the main advantage of using shorting posts is the ease in the fabrication process. Therefore, the shorting post is here considered for further performance improvement of patch quadrature coupler. However, the design consideration for a radiator is different from that for a circuit, the existing design theory cannot be applied directly on the patch quadrature coupler.

In this article, different configurations of a patch loaded with shorting posts are proposed for the implementation of quadrature coupler with loose coupling. First, the limitation of the conventional patch quadrature is investigated. After that, the centrally shorted patch configuration is proposed to widen the bandwidth together with the theoretical analysis based on the lumped equivalent circuit. Throughout this work, the bandwidth of 10 dB patch quadrature coupler can be extended to 29%, which is around 6 times of that for conventional configuration. Finally, a new patch configuration which combines four shorting posts provides superior performance in coupling coefficient range. The coupling coefficient is extended to 15 dB, which cannot be implemented using conventional configuration.